hcp metal nanoclusters with hexagonal *A*-*A* bilayer stacking stabilized by enhanced covalent bonding

S. F. Li,[1] Haisheng Li,[1] Xinlian Xue,[1] Yu Jia,[1] Z. X. Guo,[2] Zhenyu Zhang,[3,4,5] and X. G. Gong[6]
[1]*School of Physics and Engineering, Zhengzhou University, Zhengzhou 450052, China*
[2]*Department of Chemistry, University College London, London WC1H 0AJ, United Kingdom*
[3]*Materials Science and Technology Division, Oak Ridge National Laboratory, Oak Ridge, Tennessee 37831, USA*
[4]*Department of Physics and Astronomy, The University of Tennessee, Knoxville, Tennessee 37996, USA*
[5]*ICQD, University of Science and Technology of China, Hefei, Anhui, China*
[6]*MOE Key Laboratory for Computational Physical Sciences, Department of Physics, Fudan University, Shanghai 200433, China*
(Received 30 May 2010; revised manuscript received 9 July 2010; published 29 July 2010)

First-principles total energy calculations within density functional theory have been performed to study the geometric and electronic structures of Ru_n nanoclusters of varying size n ($14 \leq n \leq 42$). Strikingly, for the size range of $n=14$ to 38, the clusters always prefer a hexagonal bilayer structure with *A*-*A* stacking, rather than some of the more closely packed forms, or bilayer with *A*-*B* stacking. Such an intriguing "molecular double-wheel" form is stabilized by substantially enhanced interlayer covalent bonding associated with strong *s*-*d* hybridization. Similar *A*-*A* stacking is also observed in the ground states or low-lying isomers of the clusters composed of other hcp elements, such as Os, Tc, Re, and Co. Note that these "molecular double-wheels" show enhanced chemical activity toward H_2O splitting relative to their bulk counterpart, implying its potential applications as nanocatalysts.

DOI: 10.1103/PhysRevB.82.035443 PACS number(s): 73.22.−f, 36.40.−c, 61.46.Bc

Since the discovery of fullerenes[1] and their subsequent bulk synthesis,[2] the structure and stability of nanoclusters have been the subjects of intensive study. One motivating factor is that such nanoclusters may exhibit novel and exotic structures in contrast to their bulk counterparts, thereby offering opportunities for elucidating new types of chemical bonding. These forms of clusters and/or cluster-assembled materials, in turn, may possess unique physical and chemical properties with potential applications, e.g., in energy storage, sensing, spintronics, and catalysis. As an example, C_{60} may serve as a high-capacity medium for hydrogen storage upon Ca coating, due to strong electrostatic polarization and enhanced binding of molecular hydrogen.[3] Au prefers an fcc structure in bulk form, but due to relativistic effects Au_n clusters prefer planar, cagelike, or core-shell structures when n is small,[4,5] and such open structures of gold may exhibit outstanding catalytic properties.[6] Despite the predominance of three-dimensional structures found in bulk boron and its compounds,[7] eight- and nine-atom boron clusters are perfectly planar molecular wheels with double (σ and π) aromaticity,[8] attributed to their extreme coordination environments.

Recently, considerable attention has been paid to the structural properties of clusters of hcp and fcc transition metals (TM), a class of elements with important catalytic and magnetic applications.[4–6,9–13] In particular, it was found that Ru_n clusters of sizes ($2 \leq n \leq 13$) prefer a simple cubic structure, rather than the icosahedral-like (I_h) or buckled biplanar (BBP) structures (Ref. 9) predicted for related systems. Additionally, Co_n clusters of sizes ($13 \leq n \leq 23$) were shown to prefer multilayer structures with fcc or hcp stacking, and the enhanced stability of the layerlike structure was attributed to enhanced magnetization of the systems.[11]

In this paper, we report the discovery of a and unexpected structural form of hcp metal nanoclusters, the hexagonal bilayer structure with *A*-*A* stacking, as revealed by first-principles studies of Ru_n clusters of varying size n ($14 \leq n \leq 42$). We identify that, for the whole size range of $n=14$ to 38, the clusters always prefer the hexagonal bilayer structure with *A*-*A* stacking, rather than some of the more closely packed forms, or a bilayer with *A*-*B* stacking. We further attribute the stabilizing force of the intriguing "molecular double-wheel" structure to the substantially enhanced interlayer covalent bonding associated with strong *s*-*d* hybridization. Similar *A*-*A* stacking is also observed in the ground states or low-lying isomers of the clusters composed of other hcp elements, such as Os, Tc, Re, and Co. These findings may have broad applicability in the areas of atomic binding, nanostructure formation, nanocatalysis, and molecular devices.

Our calculations are carried out using density-functional theory (DFT)[14] with the spin-polarized generalized gradient approximations (GGA),[15] as implemented in the VASP code.[16] The wave functions are expanded in a plane wave basis with an energy cutoff of 213.3 eV. The interaction of valence electrons with the core is described with projector augmented wave (PAW) method.[17] The atomic positions are optimized with the energy convergence up to 0.001 eV. We use a simple cubic supercell with large size of 18–23 Å to make the interactions between the cluster and its periodic images negligible. Only the Γ point is used in the summation of the Brillouin zone of the simulation cell. The accuracy of the present calculation was checked by calculating the bond length of Ru_2 dimer and the lattice constant of Ru bulk. The present PAW pseudopotential method can correctly predict the binding properties of the dimer and the bulk. Simulated annealing and conjugate gradient method were used to optimize the global structures.

We performed theoretical calculations on a wide variety of structures for Ru_n ($n=14-42$) in search of the

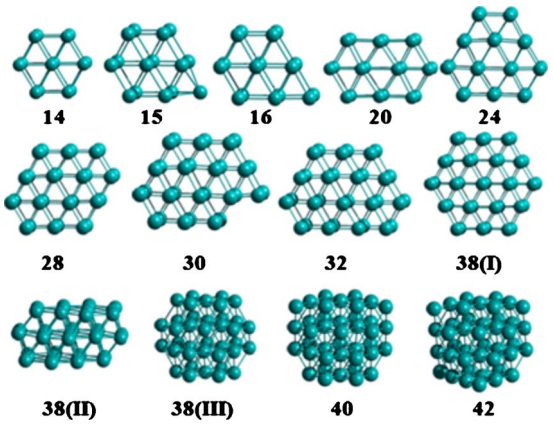

FIG. 1. (Color online) Ground-state and low-lying structures of Ru_n clusters ($n=14-42$).

global minimum, including the icosahedral-like and nonicosahedral-like structures of other species such as the recently reported Co_n (Ref. 11) and some metastable closely packed configurations from the simulated annealing method implemented by empirical potential.[18]

The ground-state structures and some low-lying isomers of Ru_n ($n=14-38$) are shown in Fig. 1. It is clear that up to $n=38$, the even-sized Ru_n clusters prefer bilayer hexagonal structures in *A-A* sequence, which are subsequently termed as the *A-A* structure. Figure 2(a) compares the average binding energies, $E_b/\text{atom}=-[E(\text{Ru}_n)-nE(\text{Ru}_{\text{atom}})]/n$, of the *A-A* structures and those of the most stable low-lying isomers with hcp/fcc multilayered (ML) fragments. The total energy difference is typically larger than 1.333 eV, except for Ru_{34}, where the *A-A* structure is more stable by 0.086 eV. The largest total energy difference is 4.535 eV for Ru_{20}. From Ru_{40}, closely packed ML structures are favored (Fig. 1) and the *A-A* structures become low-lying isomers. Here, we note that for the low-lying isomers (except for Ru_{14} and Ru_{15} preferring bilayer *A-B* structures) up to Ru_{38}, trilayer structures of hcp/fcc fragments are favored. For odd-sized clusters within the range of ($n=15-37$), the structures can be simply obtained by placing the extra atom at the outer edge of the even-sized structures of size ($n-1$).

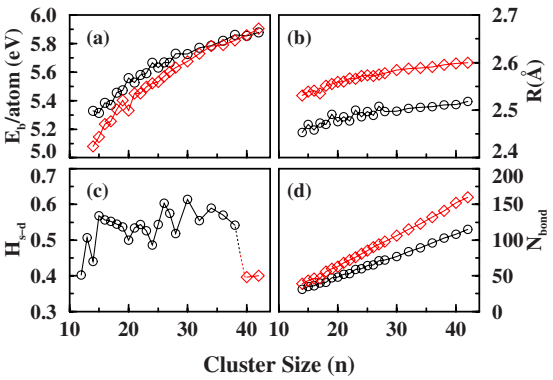

FIG. 2. (Color online) (a) Average binding energy of Ru_n clusters, E_b/atom (eV). (b) Average bond length, R(Å). (c) Calculated *s-d* hybridization index, H_{s-d}. (d) Total bond numbers, N_{bond}. Black circles: Structures arranged in *A-A* stacking; red diamonds: Structures arranged in other closely packed layered configurations.

Now, we address the detailed properties of the *A-A* structures and the structural evolution from the *A-A* sequence to ML closely packed. In the bilayer hexagonal Ru_{14} cluster presented in Fig. 1, all the bond lengths in the hexagonal plane are 2.524 Å, and the layer-layer distance is 2.203 Å. As mentioned, Co_n clusters (Ref. 11) are also identified to exhibit a layerlike structure, but our calculations show that the *A-A* structure of Ru_{14} is 3.481 eV more stable than the bilayer (*A-B*) structure of Co_{14}. It is also found to be 4.769 eV more stable than the form obtained directly from the addition of a Ru atom on the I_h-Ru_{13} unit, though this is indeed the ground state for many other TM_{14} species. As noted earlier, our previous results show that small Ru_n clusters ($n=2-13$) (Ref. 9) favor the cubic growth mode, and the Ru_{13} cluster shows a low-symmetry relaxed by the capping of one Ru atom on the surface of the Ru_{12} cuboid (Ref. 9). Ru_{15} can be obtained by capping one Ru atom on the rectangular facet (other sites are much higher in energy) of the *A-A* Ru_{14} structure, forming four equilateral bonds of 2.56 Å in length, and the bilayer *A-A* hexagonal Ru_{14} unit is well maintained.

The addition of one dimer on the rectangular facet of Ru_{14} yields the most stable Ru_{16} with a bilayer *A-A* structure, Fig. 1. When compared to Ru_{15} with an average bond length, $R=2.470$ Å, Ru_{16} shows a slightly reduced R of 2.458 Å, implying an enhanced binding energy and stability (the enhanced stability is indicated by the second-order difference of the total energy with respect to cluster size). This even-odd variation in stability also agrees well with the stability oscillations observed in smaller Ru_n clusters ($n=2-13$) reported recently (Ref. 9). Thus, in later sections we focus on the representative even-sized cases.

By symmetrically growing a Ru_2 dimer on Ru_{16}, the ground state of Ru_{18} is obtained with an *A-A* stacking. The ground state of Ru_{20} is identified to result from the simple addition of another Ru_2 dimer to the *A-A* Ru_{18}, Fig. 1, which can be seen as two hexagonal bilayer *A-A* building blocks (14-atoms) penetrating into each other with the R slightly extended to 2.476 Å, as compared with 2.453 Å of Ru_{14}. In fact, if one Ru atom rather than a Ru_2 dimer is added on the same site of Ru_{18}, the most stable structure of Ru_{19} is obtained, which is about 4.532 eV more stable than a closely packed structure relaxed upon two I_h units penetrating into each other. Furthermore, the ground-state *A-A* structure of Ru_{19} is found to be 1.366 eV more stable than a trilayer configuration with a perfect regular octahedron of the O_h symmetry, which was verified as the ground state of Co_{19} (Ref. 11).

From $n=22$ to 38, the growth of the Ru_n clusters follows a perfect hexagonal bilayer *A-A* framework upon the Ru_{14} core unit, as shown in Fig. 1. We have also calculated a wide variety of other structures and found that the hcp/fcc-like fragment structures possess significantly higher energies, typically by 3.464 eV in Ru_{24}. The cubic growth mode in small Ru_n (Ref. 9) and Rh_n,[12] as well as the I_h structures in other TM_n (Refs. 11–13), are also both significantly unfavorable. However, as the cluster size increases, the energy difference between the *A-A* structures and the most stable low-lying ML structures becomes small, as seen in Fig. 2(a). The largest cluster of a perfect hexagonal *A-A* configuration is Ru_{38}, which is about 1.451 eV more stable than the most

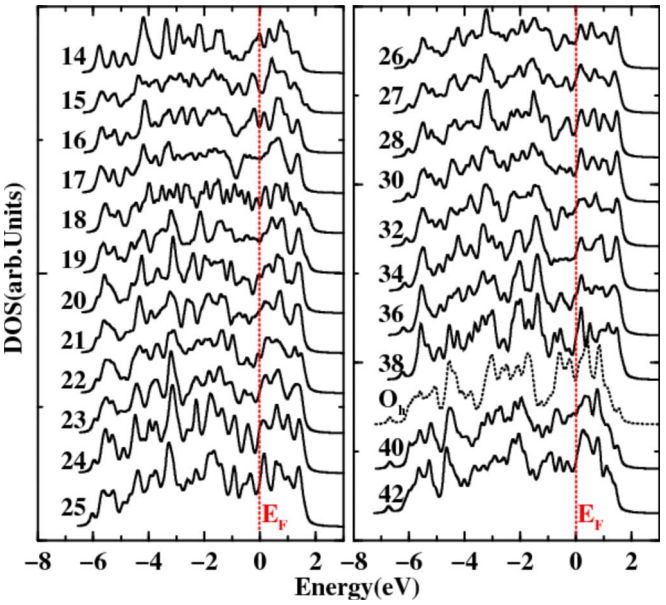

FIG. 3. (Color online) Total electronic density of states (DOS) of the ground state Ru_n. For Ru_{38}, the DOS of an O_h isomer is also provided. Fermi energy (E_F) has been shifted to zero.

stable trilayer fcc fragment with an atomic packing of 12–14–12,as shown in Fig. 1. 38(II). The *A-A* Ru_{38} is also 2.291 eV more stable than a perfect octahedron, 38(III), which has also been found as the ground-state of many other TM_{38} clusters, such as Co_{38} (Ref. 11) and Ni_{38}.[13]

We find that the *A-A* stacking is preferred only until Ru_{38}. For Ru_{40}, a more stable structure is formed by placing one Ru atom on each of two neighboring (100) facets of the O_h-Ru_{38} structure (as shown in Fig. 1), which is about 0.228 eV more stable than the bilayer *A-A* structure. Addition of two more Ru atoms on the subsequent (100) facets of the octahedron yields an optimized ground-state structure of Ru_{42}, Fig. 1. Relative to the most stable *A-A* stacking, the energy difference is raised to 1.174 eV, showing a significant structural transition from bilayered *A-A* to multilayered closely packed stacking. We also note that compared to Co_n clusters, these Ru_n clusters possess significantly small magnetic moments (MM) and the MM decreases with increasing the cluster size except for Ru_{15}, which displays the largest MM of 9.82 μB; Ru_n (n=18, 26, 30, 38, and 40) clusters carry negligible magnetism and the other clusters under present study show an MM from 2.0 to 4.0 μB with negligible magnetic energies (Ref. 11).

The total electronic density of states (DOS) of the Ru_n clusters (n=14–42) are presented in Fig. 3, which shows high peaks near the Fermi energy (E_F), indicating metallic properties and highly catalytic tendencies. Here, we also note that Ru_n clusters begin to exhibit metallic properties from $n \sim 10$, see Ref. 9. For small sizes, the even-sized clusters with a perfect *A-A* bilayer structure display simple DOS, Fig. 3, with clear sharp peaks, e.g., for Ru_{14}(Ru_{16}), compared with Ru_{15}(Ru_{17}). Ru_{18} possesses more complex DOS than both Ru_{19} and Ru_{20}, due to the geometric effect, i.e., its imperfect hexagonal *A-A* bilayer stacking. From Ru_{20} to Ru_{28}, sharp peaks occur at about 3.0 eV below the E_F, due to symmetric growth of the bilayer structure, particularly in the case of Ru_{24} and Ru_{28}. From Ru_{30}, the peaks at −3.0 eV are gradually broadened; however, peaks at about −5.6 eV become much more distinguished. For the cases of Ru_{34} to Ru_{38}, there are two sharp peaks at about −1.5 and −2.0 eV, particularly for Ru_{38} with a highly symmetric hexagonal *A-A* bilayer structure. Ru_{40} possesses similar DOS to that of Ru_{42} due to their very similar close-packed structures; however, it is evidently different from the DOS of Ru_{38}, strongly suggesting a change in their geometric structures. We stress that the profile of the DOS (the dotted) of an O_h-Ru_{38} is significantly different from that of the ground state structure of a bilayer *A-A* stacking (solid lines), due to considerable difference in their structures. We also note that the anions of all the studied Ru_n clusters maintain almost the same configurations as their neutral counterparts, leading to similar DOSs in both cases, which may be valuable for further experimental verification of these structures, such as by photoelectron spectrometry.

These hexagonal-like *A-A* bilayer structures, particularly for the cases of Ru_{14} and Ru_{38}, can be viewed as "molecular double-wheel" structures: the former and the latter possess atomic packing of 7–7 and 19–19, respectively. In each single-wheel, the bonding between the central Ru atoms and the outer rings can be viewed as "spokes" of the molecular wheels. One intriguing question is why these clusters adopt such an unusual *A-A* stacking. To answer this question, we first analyze the bonding properties of the *A-A* structures. The results are shown in Fig. 2(b). The *A-A* structures always possess shorter R by about 0.1 Å relative to other ML structures and the layer-layer distances are significantly shorter than the bonding lengths in each layer, indicating significant covalent characteristics in these *A-A* structures though the DOSs in Fig. 3 reveal metallic characteristic.

The enhanced covalency is further supported by the electronic charge-difference ($\Delta\rho$) analysis defined by $\Delta\rho = \rho(\mathrm{SC}) - \rho(\mathrm{SP})$. Here, ρ(SC) is obtained by a self-consistent calculation and ρ(SP) by the superposition of the atomic charge for the same structure. First, taking the *A-A* Ru_{14} as an example, the three-dimensional (3D) $\Delta\rho$ pattern as inserted in Fig. 4(a) reveals that the in-layer Ru atoms display evident covalent bonding, i.e., the "spokes" are of covalent nature. To further analyze the covalent bonding nature of the interlayer and perform comparisons between different sizes and structures, we have also calculated $\Delta\rho$ along the axis of the bonds between the two layers, i.e., we summed all the line $\Delta\rho$ together along the axis of the bonds between the two layers and then divided by the number of bonds. As presented in Fig. 4(a), charge density accumulates considerably at the bond center, revealing a significant level of covalent bonding of the interlayer. With the size decreases from infinite 3D *A-A* Ru bulk through *A-A* Ru_{38} to *A-A* Ru_{14}, the covalent bonding of the interlayer becomes stronger and stronger. We also stress that for the cases of a bilayer *A-B* Ru_{14} isomer and hcp Ru bulk, the covalent bonding of the interlayers are considerably weaker than those of the "molecular double-wheel," implying the unique bonding properties in these unusual nanostructures. To support the strong covalent bonding in these Ru_n nanostructures, we also select an *A-A* Mg_{38} isomer (the ground state O_h-Mg_{38} is about

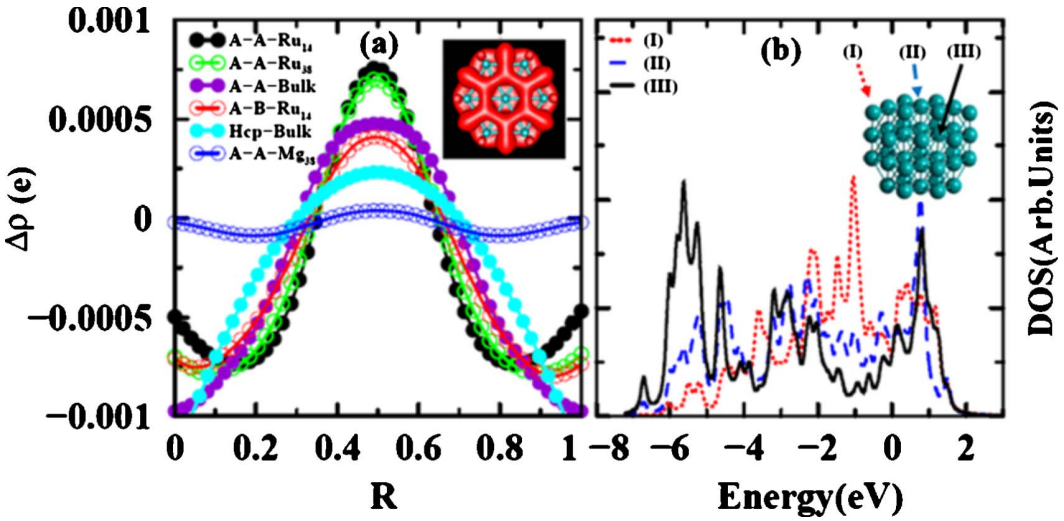

FIG. 4. (Color online) (a) Averaged charge density differences, $\Delta\rho$, along the axis of the bonds of the interlayer for different systems; the bond lengths are shown in normalized scale; the insert is the three-dimensional $\Delta\rho$ for Ru_{14}. (b) The local projected density of states of the O_h-like Ru_{40} structure for corner (red dotted), face-center (blue dashed) and center atoms (black solid line), respectively.

4.945 eV more stable) for comparison, and one can see that there is a negligible peak in the line $\Delta\rho$. Although bulk Mg possesses an hcp structure, due to the weak covalent bonding nature, Mg_n clusters within the current size range still prefer the close packed structure[19] rather than the *A*-*A* packing.

The competition between the covalent bonding and the coordination number determines the structural evolution from *A*-*A* to ML configurations. For a given cluster, its stability depends on both the average bonding strength and the total number of the bonds (N_{bond}) involved. In Fig. 2(c), we present the *s*-*d* hybridization indices, $H_{s\text{-}d}$ (for definition, see Ref. 9), of the ground-state structures of Ru_n clusters. Evidently, the $H_{s\text{-}d}$ values of the *A*-*A* Ru_n clusters (n=14–38) are considerably larger than those of the smaller Ru_{12} and larger Ru_n clusters (n=40 and 42), indicating a stronger binding in the former cases. Figure 2(d) presents the N_{bond} as a function of cluster size. Clearly, in the small size range, the number of bonds in *A*-*A* structures is comparable with that of the multilayer fcc or hcp fragments, thus the *A*-*A* growth mode is preferred due to relatively strong covalent bonding. With increasing cluster size, the number of bonds in ML structure dramatically increases relative to that of *A*-*A* structure, mainly as a result of the increased number of encapsulated atoms. These encapsulated inner atoms [type III atoms in Fig. 4(b)] have a higher coordination number and possess larger binding energies, subsequently lowering the total energy, as implied by the much enhanced (reduced) peaks in the deep (shallow) energy levels in the local projected DOS of the O_h-like Ru_{40} [see Fig. 4(b)]. We also note that the covalent bonding is gradually weakened with the increasing size, and the metallic bonding begins to dominate the stability. Thus beyond a critical size (n=38), more closely packed ML fragments become more stable.

We have also checked the stabilities of the *A*-*A* structure for some other hcp transition-metal elements near Ru in the periodic table. We find that almost all the Os_n clusters in the current studied size range also prefer the *A*-*A* stacking, by a typical energy difference of 0.363 eV for Os_{40}, if compared to that of other stacking forms (such as *A*-*B*, *A*-*B*-*A*, or *A*-*B*-*C*). For smaller Tc_n clusters, structures with *A*-*A* stacking are essentially degenerate in energy compared with those of other closely packed structures. For Re_n and Co_n, the structures with *A*-*A* stacking are also found to be low-lying isomers. Furthermore, relatively strong covalent bonding is also clearly observed in the *A*-*A* bilayer structures of Os_n, Tc_n and the layerlike structures of Co_n (Ref. 11). However, in the current size range studied, the slightly weaker covalent bonding properties involved in Fe_n, Co_n, and Tc_n, relative to Ru_n, resulting in the low-lying isomers of *A*-*A* stacking for the former cases.

Finally, we identify that relative to their bulk counterpart, these *A*-*A* bilayer Ru_n nanostructures possess significantly enhanced chemical activities toward H_2O splitting. Recently, both dissociation and non-dissociation observations were identified for H_2O adsorption on the Ru(0001) surface,[20–24] indicating that Ru(0001) is on the border of active and inactive metal surfaces with respect to dissociation of water. The underlying essential point may be that the barrier for desorption of the nondissociated adsorbed water is comparable with the dissociation barrier[23,24] on the Ru(0001) surface. However, this observation may change in the nanoscale.

Here, we simply report the adsorption and dissociation behaviors for a H_2O molecule on Ru_{14}, the smallest double-wheel in our findings. In our calculations,[25] the optimized H_2O molecule possess R(H-O)=0.973 Å and ∠H-O-H =104.61°, in close agreement with previous calculations.[24] As presented in Fig. 5(a), we find that H_2O favors to adsorb on the top of the edge Ru atom with an adsorption energy $\{E_{ads}=-[E(H_2O/Ru_{14})\text{-}E(H_2O)\text{-}E(Ru_{14})]\}$ of 0.671 eV, bond length R(O-Ru)=2.231 Å, R(H-Ru)=0.978 Å, and ∠H-O-H=108.03°, respectively. We note that the H_2O monomer possesses a significantly larger E_{ads} on the cluster than that on the Ru(0001) surface, 0.409 eV,[24] and the enlarged ∠H-O-H along with this larger adsorption energy indicates a stronger activation of the H_2O molecule in the former case. On this site, splitting the H_2O species further

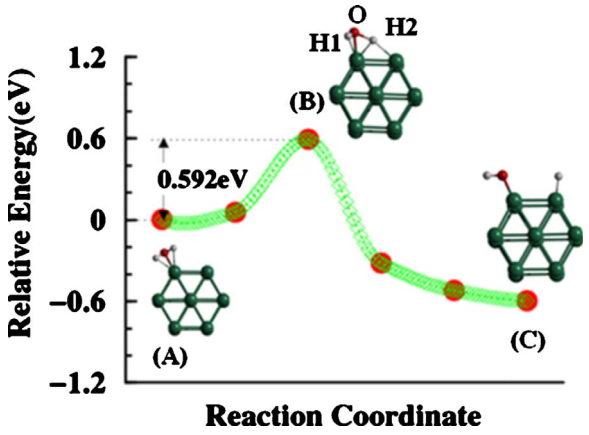

FIG. 5. (Color online) The minimum energy path (MEP) obtained by NEB calculations for a H_2O molecule dissociation on *A*-*A*-Ru_{14}. (a), (b), and (c) correspond to the favorite molecular adsorption geometry, the saddle point, and the dissociation configuration, respectively.

lowers the total energy by 0.596 eV, resulting in the configuration as shown in Fig. 5(c). Importantly, with the improved climbing image nudged-elastic-band (NEB)[26] method, we identify that the energy barrier involved in the dissociation process is only 0.592 eV [see Fig. 5(b) for the configuration of the saddle point, R(O-Ru)=2.102 Å, R(O-H1)=0.981 Å, R(O-H2)=1.332 Å, and ∠H-O-H=112.39°], which is considerably smaller than the adsorption energy of 0.653 eV, i.e., the desorption barrier. Therefore, the above results strongly suggest that these novel double-wheel Ru nanostructures possess superior chemical activity to their bulk counterpart for water splitting due to their intriguing atomic bonding and chemical properties in the nanoscale. In fact, the observed enhanced chemical activity of these Ru_n bilayer nanostructures can be readily understood from the *d* band theory.[27] Our calculations show that the *d* band center of the first-layer surface atoms of Ru(0001) simulated with a six-layer slab model is located at −1.971 eV. However, the Ru_{14} cluster possesses a *d* band center of −1.910 eV, particularly, the *d* band center of the edge atoms with less coordination numbers is even higher, −1.844 eV, in close agreement with the density of state analysis as presented in Fig. 4(b), rendering these sites are more active for molecular adsorption.

In summary, we have carried out a systematic first-principles study of the geometric and electronic structures of Ru_n clusters of varying size n ($14 \leq n \leq 42$). Our studies lead to the surprising finding that, for the size range of $n=14$ to 38, the clusters always prefer a hexagonal bilayer structure with *A*-*A* stacking, rather than some of the more closely packed structures, or bilayer with *A*-*B* stacking. The intriguing "molecular double-wheel" structure is stabilized by the substantially enhanced interlayer covalent bonding associated with strong *s*-*d* hybridization. Similar covalent-bonding stabilized *A*-*A* stacking is also observed in the ground states or low-lying isomers of clusters composed of other hcp elements, such as Os, Tc, Re, and Co. These findings, predicting the first transition-metal based "molecular double-wheel" structures, may be instrumental in the design of new forms of nanocatalysts and molecular nanodevices.

This work was supported in part by the National Science Foundation of China under Grant No. 10604049 (S.F.L.); UK EPSRC under U.K.-SHEC (Grant No. EP/E040071/1), Platform Grants (Grants No. EP/E046193/1 and No. EP/F013612/1) (Z.X.G.); the special funds for major state basic research, NSFC and Shanghai Project (G.X.G.); USNSF under Grant No. DMR-0606485, and in part by U.S. DOE (Grant No. DE-FG02-05ER46209, and the Division of Materials Sciences and Engineering, Office of Basic Energy Sciences) (Z.Y.Z.).

[1] H. W. Kroto, J. R. Heath, S. C. O'Brien, R. F. Curl, and R. E. Smalley, Nature (London) **318**, 162 (1985).
[2] W. Krätschmer, L. D. Lamb, K. Fostiropoulos, and D. R. Huffman, Nature (London) **347**, 354 (1990).
[3] M. Yoon, Shenyuan Yang, Christian Hicke, Enge Wang, David Geohegan, and Zhenyu Zhang, Phys. Rev. Lett. **100**, 206806 (2008).
[4] H. Häkkinen, Michael Moseler, and Uzi Landman, Phys. Rev. Lett. **89**, 033401 (2002).
[5] X. Gu, M. Ji, S. H. Wei, and X. G. Gong, Phys. Rev. B **70**, 205401 (2004); Yi Gao and Xiao Cheng Zeng, J. Am. Chem. Soc. **127**, 3698 (2005); W. Huang, M. Ji, C. D. Dong, X. Gu, L. M. Wang, X. G. Gong, and Lai-Sheng Wang, ACS Nano **2**, 897 (2008).
[6] M. D. Hughes, Yi-Jun Xu, Patrick Jenkins, Paul McMorn, Philip Landon, Dan I. Enache, Albert F. Carley, Gary A. Attard, Graham J. Hutchings, Frank King, E. Hugh Stitt, Peter Johnston, Ken Griffin, and Christopher J. Kiely, Nature (London) **437**, 1132 (2005).
[7] *Boron Hydride Chemistry*, edited by E. L. Muetterties (Academic Press, New York, 1975); F. A. Cotton, G. Wilkinson, C. A. Murillo, and M. Bochmann, *Advanced Inorganic Chemistry*, 6th ed. (Wiley, New York, 1999).
[8] H.-J. Zhai, A. N. Alexandrova, K. A. Birch, A. I. Boldyrev, and L.-S. Wang, Angew. Chem., Int. Ed. **42**, 6004 (2003).
[9] S. Li, H. Li, J. Liu, X. Xue, Y. Tian, H. He, and Y. Jia, Phys. Rev. B **76**, 045410 (2007); C. M. Chang and M. Y. Chou, Phys. Rev. Lett. **93**, 133401 (2004); Wenqin Zhang, Haitao Zhao, and Lichang Wang, J. Phys. Chem. B **108**, 2140 (2004), and references therein.
[10] A. J. Cox, J. G. Louderback, S. E. Apsel, and L. A. Bloomfield, Phys. Rev. B **49**, 12295 (1994).
[11] C. D. Dong and X. G. Gong, Phys. Rev. B **78**, 020409(R) (2008); J. L. Rodríguez-López, F. Aguilera-Granja, K. Michaelian, and A. Vega, *ibid.* **67**, 174413 (2003), and references therein.
[12] Y. C. Bae, H. Osanai, V. Kumar, and Y. Kawazoe, Phys. Rev. B **70**, 195413 (2004); Y. C. Bae, V. Kumar, H. Osanai, and Y. Kawazoe, *ibid.* **72**, 125427 (2005).
[13] Q.-M. Zhang, Jack C. Wells, X. G. Gong, and Zhenyu Zhang,

Phys. Rev. B **69**, 205413 (2004).
[14] W. Kohn and L. J. Sham, Phys. Rev. **140**, A1133 (1965).
[15] J. P. Perdew and Y. Wang, Phys. Rev. B **45**, 13244 (1992).
[16] G. Kresse and J. Furthmüller, Phys. Rev. B **54**, 11169 (1996); Comput. Mater. Sci. **6**, 15 (1996).
[17] P. E. Blöchl, Phys. Rev. B **50**, 17953 (1994); G. Kresse and D. Joubert, *ibid.* **59**, 1758 (1999).
[18] F. Cleri and V. Rosato, Phys. Rev. B **48**, 22 (1993).
[19] A. Lyalin, I. A. Solov'yov, A. V. Solov'yov, and W. Greiner, Phys. Rev. A **67**, 063203 (2003).
[20] P. J. Feibelman, Science **295**, 99 (2002).
[21] G. Held and D. Menzel, Surf. Sci. **316**, 92 (1994).
[22] D. N. Denzler, Ch. Hess, R. Dudek, S. Wagner, Ch. Frischkorn, M. Wolf, and G. Ertl, Chem. Phys. Lett. **376**, 618 (2003).
[23] K. Andersson, A. Nikitin, L. G. M. Pettersson, A. Nilsson, and H. Ogasawara, Phys. Rev. Lett. **93**, 196101 (2004).
[24] Sheng Meng, E. G. Wang, and Shiwu Gao, Phys. Rev. B **69**, 195404 (2004); A. Michaelides, A. Alavi, and D. A. King, J. Am. Chem. Soc. **125**, 2746 (2003).
[25] In our calculations, to obtain the adsorption energy and the dissociation path for H_2O on Ru_{14} cluster, we use PAW-PBE potential, which is generally regarded as more accurate to describe an adsorption process, though our test shows that PAW-GGA give almost the same data.
[26] G. Henkelman, B. P. Uberuaga, and H. Jónsson, J. Chem. Phys. **113**, 9901 (2000); G. Henkelman and H. Jónsson, *ibid.* **113**, 9978 (2000).
[27] Y. Xu, A. Ruban, and M. Mavrikakis, J. Am. Chem. Soc. **126**, 4717 (2004); M. Gajdos, A. Eichler, and J. Hafner, J. Phys.: Condens. Matter **16**, 1141 (2004); O. M. Lovvik and R. A. Olsen, J. Chem. Phys. **118**, 3268 (2003); A. Roudgar and A. Gross, Phys. Rev. B **67**, 033409 (2003); Y. Gauthier, M. Schmid, S. Padovani, E. Lundgren, V. Bus, G. Kresse, J. Redinger, and P. Varga, Phys. Rev. Lett. **87**, 036103 (2001); V. Pallassana and M. Neurock, J. Catal. **191**, 301 (2000); M. Mavrikakis, B. Hammer, and J. K. Nørskov, Phys. Rev. Lett. **81**, 2819 (1998).